Proceedings of IOE Graduate Conference, 2019-Summer
Peer Reviewed
Year: 2019 Month: May Volume: 6
ISSN: 2350-8914 (Online), 2350-8906 (Print)

Free Vibration Analysis of Simply Supported Pelton Turbine: A Case of Flexible Rotor Bearings

Janak Kumar Tharu [a], Nishant Bhatta [b], Sanjeev Karki [c], Mahesh Chandra Luintel [d]

Department of Mechanical Engineering, Pulchowk Campus, IOE, Tribhuvan University, Nepal
Corresponding Email: [a] janak5tharu@gmail.com, [b] nishant.bhatta205@gmail.com, [c] sanjeev1karki@gmail.com, [d] mcluintel@ioe.edu.np,

Abstract
Vibration is an important factor affecting the performance, reliability and life of the turbine. Most of the researches on vibration of Pelton turbine are mainly based on assumptions of rigid rotor bearings. This paper focuses on the free transverse vibration analysis due to flexible rotor bearings at the support ends. An analytical model is developed based on rigid foundation, flexible bearings, flexible and continuous shaft and rigid disk. The stiffness of each SKF 1206 EKTN9 + H206 self-aligning ball bearing with adapter sleeve at operating speed of 1500 rpm is computed to be 47.487 MN/m. Then this stiffness value is used in boundary conditions of non-rotating uniform shaft to determine the mode shapes. Using assumed mode method, the kinetic energies and strain energies of the shaft and the disk and non-conservative work of the bearings are then derived in the form of displacements and gradient and rate of displacements.These general expressions of the system's energies and work are substituted in Lagrange's equation of motion(EOM) to finally get the system's EOM. The solutions as the natural frequencies of vibration are determined taking first three modes. Engine order(EO) encompassing 16 number of buckets is passed from origin intersecting frequency lines so the critical frequencies are found to be 316.365, 316.373, 1972.256, 2059.466, 4845.386 and 4845.619 rpm with overestimation of 1.15%, 1.14%, 15.21%, 12.90%, 5.37% and 5.35% respectively from numerical results of modal analysis in ANSYS.

Keywords
Stiffness, mode shapes, equation of motion, critical frequencies, Campbell diagram, engine order, whirl

1. Introduction

From early days, water wheels are used to extract mechanical energy. In the 1870s, Lester Allan Pelton modified the water wheel to extract electrical energy which is now known as Pelton wheel or Pelton turbine [1]. Many factors affect the performance of the turbine. Vibration is an important factor affecting the performance, reliability and life of the turbine. If the operating speed of turbine matches with critical frequencies, resonance will occur and can cause failure [2]. Thus, the study of vibration is essential.

Very less work has been done in the field of the dynamic behavior of Pelton turbines and their effects in operation and design [3]. Most of the work done are mainly based on the vibration analysis of Pelton turbine considering rigid rotor bearings. But rotor bearings at the support are not rigid and can result in damping and stiffness effects. Considering support bearings rigid one will be very simplified and hence may not lead to accurate result.

An analytical model considering flexible rotor bearings at the supports is developed which is used to calculate natural frequencies of the system.

2. Research Methodology

For the mathematical modelling of the Pelton turbine system, the components necessary for dynamic analysis are first determined and modelled in terms of their dynamic properties. Then the stiffness of bearings are calculated which are substituted in mode shapes. The stiffness and mode shapes are then substituted in systems energies and work. The energies and work are then put into Lagrange's equation of motion to get the system's equations of motion. The equations are solved to obtain natural frequencies as the solutions. The obtained analytical results are finally compared with the numerical results from modal analysis of ANSYS. The analytical and numerical results are also plotted in the form of Campbell diagrams [4].

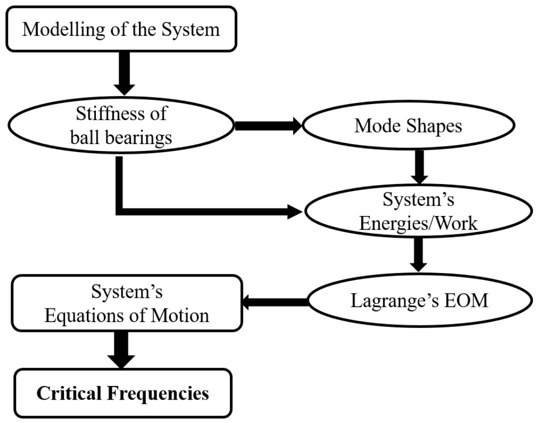

Figure 1: Research Methodology

3. Mathematical Model

Only, the transverse vibration of the system is considered ignoring the longitudinal and torsional effects. The transverse axes are X- and Y-axes while the longitudinal axis is Z-axis. The displacements in the transverse directions are u(z,t) and v(z,t).

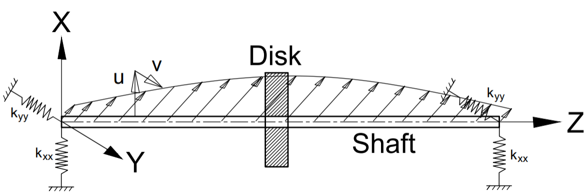

Figure 2: Modelling of the System

The rotordynamic components of Pelton turbine system are foundation, bearings, shaft and disk. The foundation is assumed to be rigid so its dynamic analysis is not required.

The bearings at the supports are taken to be flexible. The rotation of the shaft exerts radial force on the inner race. Due to this, the inner race is displaced resulting in stiffening of the rolling elements. In case of free vibration, equal radial forces act in all directions and the stiffness in both transverse directions are equal.

$$i.e.\ k_{xx} = k_{yy}$$

The variation of non-conservative work of each bearing is then given by [4]

$$\delta W_{nc} = -k_{xx} u \delta u - k_{yy} v \delta v \tag{1}$$

The shaft is assumed to be flexible and continuous so its kinetic and strain energies are [4]

$$T_S = \frac{1}{2}\rho_S A_S \int_0^{L_S} (\dot{u}^2 + \dot{v}^2) dz + \frac{1}{2}\rho_S I_{Sxx} \int_0^{L_S} (\omega_x^2 + \omega_y^2) dz + \frac{1}{2}\rho_S I_{Szz} \int_0^{L_S} \omega_z^2 dz \tag{2}$$

$$V_S = \frac{1}{2} E_S I_{Sxx} \int_0^{L_S} \left[\left(u''\right)^2 + \left(v''\right)^2 \right] dz \tag{3}$$

where $\dot{u}$ denotes the time derivative of u and u'' denotes the double derivative of u with respect to z.

The disk is considered to be a rigid lumped mass at the center of the shaft so the strain energy is negligible while its kinetic energy is [4]

$$T_D = \left[\frac{1}{2} m_D (\dot{u}^2 + \dot{v}^2) + \frac{1}{2} I_{Dxx} (\omega_x^2 + \omega_y^2) + \frac{1}{2} I_{Dzz} \omega_z^2 \right]_{z=L/2} \tag{4}$$

3.1 Stiffness of bearings

The bearings for the given system are SKF self-aligning ball bearings with an adapter sleeve. The designation is 1206 EKTN9 + H206. The following formulae have been adapted from [5]

External radial force $(F_{ex}) = k_r \left(\frac{\nu N}{1000}\right)^{2/3} \left(\frac{d_m}{100}\right)^2$

Load zone $(\psi_l) = cos^{-1}\left(\frac{c_r}{x_m cos(\gamma)}\right)$

Contact deformation $\delta(\psi) = x_m cos(\gamma) cos(\psi) - c_r$

Compressive load $F(\psi) = k_{pio} \delta^{3/2}$

Internal radial force $(F_{in}) = \sum_{j=1}^{Z} F(\psi_j)$

Stiffness $(k_b) = 1.5 \frac{Z}{4.37} cos(\gamma) k_{pio} [x_m cos(\gamma) - c_r]^{0.5}$

Following parameters have been taken from SKF bearing catalogue.

Table 1: Bearing Parameters

SN	Parameters	Values
1	Minimum load factor (k_r)	0.04
2	Number of balls (Z)	28
3	Internal radial clearance (c_r)	0.033 mm
4	Viscosity of lubricant (ν)	70 mm^2/s

Table 2: Calculated Parameters

SN	Parameters	Units	Values
1	d_m	mm	46
2	γ	degrees	8.35
3	k_{pio}	kN/$mm^{1.5}$	49.073

Where, d_m = bearing mean diameter, γ = position of ball element with respect to vertical, k_{pio} = deformation constant

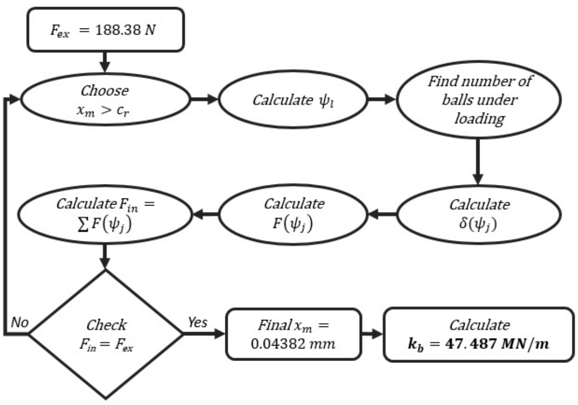

Figure 3: Stiffness of bearings

For operational speed of 1500 r/min, the external radial force is calculated to be 188.38 N. This force causes the displacement of inner race alongwith deformation of the ball elements. The external force is balanced by stiffening of certain number of ball elements. To balance the external and internal forces, a value of displacement ($x_m > c_r$) is chosen and load zone is calculated along with number of ball elements under loading. The contact deformation of each loaded ball element is calculated and correspondingly the compressive force felt by each ball is also calculated. These forces are summed up to match external force. If the forces are not balanced, another value of x_m is chosen and the process is repeated until the forces are balanced [5].

As shown in figure 3, after a number of trials, the final value of x_m is found to be 0.04382 mm which gives the stiffness value to be 47.487 MN/m.

3.2 Mode Shapes

The mode shape for free transverse vibration of a non-rotating uniform shaft element is given by [6]

$$\begin{aligned} U(z) =& Acos(\beta z) + Bsin(\beta z) \\ &+ Ccosh(\beta z) + Dsinh(\beta z) \end{aligned} \tag{5}$$

With boundary conditions:

$$Moments:\ E_S I_{Sxx} \frac{\partial^2 U}{\partial z^2} = 0;\ at\ z = 0\ and\ z = L_S \tag{6}$$

$$\begin{aligned} Shear\ Forces:\ E_S I_{Sxx} \frac{\partial^3 U}{\partial z^3} &= a k_b U;\ a = -1\ at\ z = 0 \\ and\ a &= +1\ at\ z = L_S \end{aligned} \tag{7}$$

Using boundary conditions (6) and (7) in expression (5), four equations are obtained which after solving give the frequency equation.

$$\begin{aligned} &\frac{sin(\beta L_S) + \alpha[cos(\beta L_S) - cosh(\beta L_S)]}{sinh(\beta L_S) + \alpha[cos(\beta L_S) - cosh(\beta L_S)]} \\ &= \frac{[2\alpha cosh(\beta L_S) - sinh(\beta L_S)] - 2\alpha^2 M + \alpha P}{[2\alpha cos(\beta L_S) + sin(\beta L_S)] - 2\alpha^2 M + \alpha P} \end{aligned} \tag{8}$$

where $\alpha = \frac{E_S I_{Sxx}}{2k_b}\beta^3$; $M = [sin(\beta L_S) + sinh(\beta L_S)]$; $P = [cos(\beta L_S) + cosh(\beta L_S)]$

The values for the model are:

$E_S I_{Sxx} = 10.397 kNm^2$; $L_S = 0.519 m$

Cross multiplying equation (8) and making RHS zero, the frequency expression is obtained which after plotting gives infinite values of β.

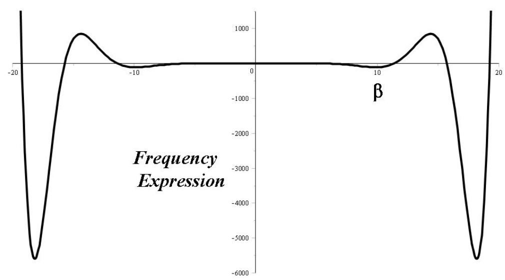

Figure 4: Frequency equation plot

The mode shape (5) then converts to

$$\begin{aligned} U_n(z) =& sin(\beta_n z) + m_n sinh(\beta_n z) \\ &+ \alpha_n(1 - m_n)[cos(\beta_n z) + cosh(\beta_n z)] \end{aligned} \tag{9}$$

where

$$m_n = \frac{sin(\beta_n L_S) + \alpha_n[cos(\beta_n L_S) - cosh(\beta_n L_S)]}{sinh(\beta_n L_S) + \alpha_n[cos(\beta_n L_S) - cosh(\beta_n L_S)]}$$

The values of β_n, α_n and m_n for three modes are given in table 3:

Table 3: Mode Shape Parameters

Modes (n)	β_n	α_n	m_n
1	5.9619	0.0232	-0.0216
2	11.3744	0.1611	-0.1933
3	15.7109	0.4245	-0.7370

The first three mode shapes from analytical results are in figure 5:

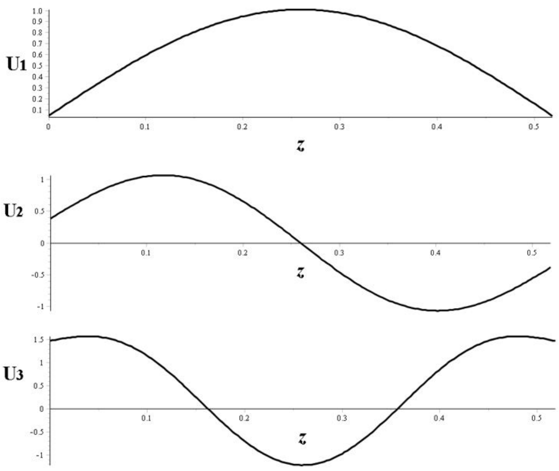

Figure 5: First three mode shapes

The modal analysis results from Analysis Systems (ANSYS) are shown in figure 6:

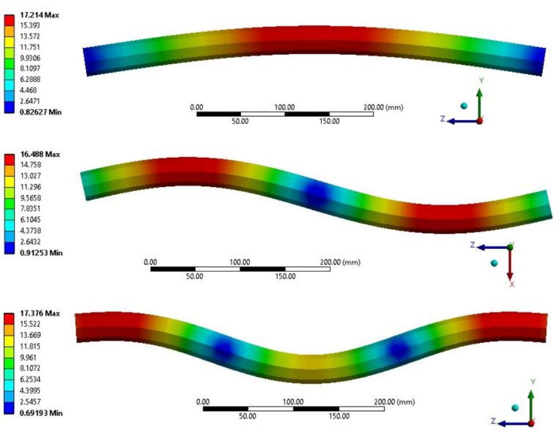

Figure 6: First three mode shapes from ANSYS

From figures (5) and (6), the mode shapes results from analytical model and ANSYS model are in good approximation with each other.

The values of higher mode shapes at the boundaries are higher because at higher modes, α is higher and the bearing stiffness(k_b) at the boundaries is no longer able to fully sustain the shaft stiffness($E_S I_{Sxx} \beta^3/2$).

For the simplification of energy expressions, following conditions of the mode shapes can be used.

For $i \neq j$,

$$\int_0^{L_S} U_i U_j dz = 0$$

$$\int_0^{L_S} \frac{d^2U_i}{dz^2}\frac{d^2U_j}{dz^2} dz = -\frac{k_b}{E_S I_{Sxx}}[U_i U_j(0) + U_i U_j(L_S)] \tag{10}$$

About $z = L_S/2$ (where the disk is located),

$$\begin{aligned} U_n(z) &= \ even\ function\ for\ odd\ n \\ U_n(z) &= \ odd\ function\ for\ even\ n \end{aligned} \tag{11}$$

At $z = L_S/2$,

$$\begin{aligned} U_n(z) &= 0\ for\ even\ n \\ \frac{dU_n}{dz}(z) &= 0\ for\ odd\ n \end{aligned} \tag{12}$$

With $k_b \rightarrow \infty$, the case becomes that of rigid rotor bearings and the mode shape equation (9) converts to $sin(\pi z/L_S)$ which is in accordance with the mode shape for rigid bearings found in [7].

3.3 System's Energies and Work

The final frame of reference gained by disk and shaft is through a sequence of rotations given by a set of Euler angles 123. The rotations are about X-, Y- and Z-axes in order [8].

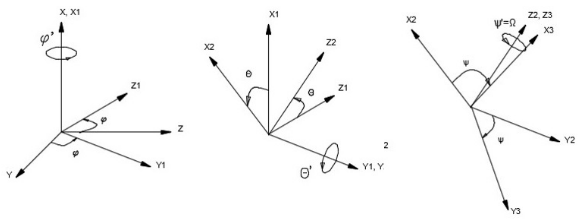

Figure 7: Rotation angles achieved by disk and shaft

The rotational speed of the shaft and disk is [4]

$$\omega = \dot{\phi}X + \dot{\theta}Y_1 + \dot{\psi}Z_2$$

where X, Y_1 *and* Z_2 denote unit vectors along X, Y1 and Z2 axes

$$\left\{\begin{array}{c}\omega_x\\ \omega_y\\ \omega_z\end{array}\right\}=\left\{\begin{array}{c}\dot{\phi}cos\psi cos\theta+\dot{\theta}sin\psi\\ -\dot{\phi}sin\psi cos\theta+\dot{\theta}cos\psi\\ \dot{\phi}sin\theta+\dot{\psi}\end{array}\right\}$$

Since $\theta\approx 0,\ \phi\approx 0,\ sin\theta\approx\theta\ and\ cos\theta\approx 1$

$$\therefore\left\{\begin{array}{c}\omega_x\\ \omega_y\\ \omega_z\end{array}\right\}=\left\{\begin{array}{c}\dot{\phi}cos\psi+\dot{\theta}sin\psi\\ -\dot{\phi}sin\psi+\dot{\theta}cos\psi\\ \dot{\phi}\theta+\dot{\psi}\end{array}\right\} \tag{13}$$

Since the mode shapes in both transverse directions are same in the case of free vibration as the stiffness of bearings are equal in both directions. Using assumed mode method [9], the transverse displacements are in the form of

$$\begin{aligned}u(z,t)&=\sum_{n=1}^{\infty}U_n(z)q_{un}(t)\\ v(z,t)&=\sum_{n=1}^{\infty}U_n(z)q_{vn}(t)\end{aligned} \tag{14}$$

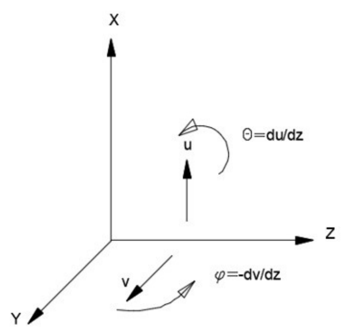

Figure 8: Relation between angular and transverse displacements

The angular and transverse displacements are related as [4]

$$\begin{aligned}\phi&=-\frac{\partial v}{\partial z}=-\sum_{n=1}^{\infty}\frac{\partial U_n}{\partial z}(z)\ q_{vn}(t)\\ \theta&=\frac{\partial u}{\partial z}=\sum_{n=1}^{\infty}\frac{\partial U_n}{\partial z}(z)\ q_{un}(t)\end{aligned} \tag{15}$$

After substitutions of relations (13) to (15) in the energy and work expressions (1) to (4) and use of conditions (10) to (12),

The energy expressions (2) and (3) become

$$\begin{aligned}T_S=&\frac{1}{2}\rho_S A_S\int_0^{L_S}\sum_{n=1}^{\infty}(U_n(z))^2\left[(\dot{q}_{un}(t))^2+(\dot{q}_{vn}(t))^2\right]dz\\ &+\frac{1}{2}\rho_S I_{Sxx}\int_0^{L_S}\left[\sum_{n=1}^{\infty}\left(U_n'(z)\dot{q}_{un}(t)\right)^2\right.\\ &\left.+\sum_{n=1}^{\infty}\left(U_n'(z)\dot{q}_{vn}(t)\right)^2\right]dz+\frac{1}{2}\rho_S I_{Szz}\Omega^2 L_S\\ &-\rho_S I_{Szz}\Omega\int_0^{L_S}\left(\sum_{n=1}^{\infty}U_n'(z)q_{un}(t)\right)\left(\sum_{n=1}^{\infty}U_n'(z)\dot{q}_{vn}(t)\right)dz\end{aligned} \tag{16}$$

And

$$\begin{aligned}V_S=&\frac{1}{2}E_S I_{Sxx}\int_0^{L_S}\sum_{n=1}^{\infty}\left(U_n''(z)\right)^2\left[(q_{un}(t))^2+(q_{vn}(t))^2\right]dz\\ &-\frac{1}{2}k_b\sum_{i\neq j}^{\infty}[U_iU_j(0)+U_iU_j(L_S)]q_{ui}(t)q_{uj}(t)\\ &-\frac{1}{2}k_b\sum_{i\neq j}^{\infty}[U_iU_j(0)+U_iU_j(L_S)]q_{vi}(t)q_{vj}(t)\end{aligned} \tag{17}$$

The kinetic energy of the disk (4) converts to

$$\begin{aligned}T_D=&\frac{1}{2}m_D\left[\left(\sum_{odd\ n}^{\infty}U_n(z)\dot{q}_{un}(t)\right)^2\right.\\ &\left.+\left(\sum_{odd\ n}^{\infty}U_n(z)\dot{q}_{vn}(t)\right)^2\right]_{z=L_S/2}\\ &+\frac{1}{2}I_{Dxx}\left[\left(\sum_{even\ n}^{\infty}U_n'(z)\dot{q}_{vn}(t)\right)^2\right.\\ &\left.+\left(\sum_{even\ n}^{\infty}U_n'(z)\dot{q}_{un}(t)\right)^2\right]_{z=L_S/2}+\frac{1}{2}I_{Dzz}\Omega^2\\ &-I_{Dzz}\Omega\left(\sum_{even\ n}^{\infty}U_n'(z)\dot{q}_{vn}(t)\right)\\ &\left(\sum_{even\ n}^{\infty}U_n'(z)q_{un}(t)\right)_{z=L_S/2}\end{aligned} \tag{18}$$

With the use of $k_b=k_{xx}=k_{yy}$, the variation of the non-conservative work of the bearings (1) becomes

$$\begin{aligned}\delta W_{nc} = & -k_b \sum_{i=1}^{\infty} (U_i(0))^2 [q_{ui}(t)\delta q_{ui}(t) + q_{vi}(t)\delta q_{vi}(t)] \\ & - k_b \sum_{i=1}^{\infty} (U_i(L_S))^2 [q_{ui}(t)\delta q_{ui}(t) + q_{vi}(t)\delta q_{vi}(t)] \\ & - k_b \sum_{i\neq j}^{\infty} [U_i U_j(0) + U_i U_j(L_S)] q_{ui}(t)\delta q_{uj}(t) \\ & - k_b \sum_{i\neq j}^{\infty} [U_i U_j(0) + U_i U_j(L_S)] q_{vi}(t)\delta q_{vj}(t)\end{aligned} \tag{19}$$

3.4 Equations of Motion

The Lagrange's equation of motion is given by [10]

$$\frac{d}{dt}\left(\frac{\partial L}{\partial \dot{q}_{rs}}\right) - \frac{\partial L}{\partial q_{rs}} = \frac{\partial W_{nc}}{\partial q_{rs}}$$

where $r = u, v$ represents the directions of transverse displacement, $s = 1, 2, ...$ represents the mode shape

And Lagrangian $(L) = T - V$

$$\begin{aligned}\therefore \frac{d}{dt}\left(\frac{\partial T_D}{\partial \dot{q}_{rs}} + \frac{\partial T_S}{\partial \dot{q}_{rs}} - \frac{\partial V_S}{\partial \dot{q}_{rs}}\right) - \frac{\partial T_D}{\partial q_{rs}} \\ - \frac{\partial T_S}{\partial q_{rs}} + \frac{\partial V_S}{\partial q_{rs}} = \frac{\partial W_{nc}}{\partial q_{rs}}\end{aligned} \tag{20}$$

Substituting the expressions (16) to (19) into (20), the system's EOMs are

$$\begin{aligned}& \sum_{odd\ n}^{\infty} \left[m_D U_S\left(\frac{L_S}{2}\right) U_n\left(\frac{L_S}{2}\right)\right] \ddot{q}_{un}(t) \\ & + \sum_{even\ n}^{\infty} \left[I_{Dxx} U_S'\left(\frac{L_S}{2}\right) U_n'\left(\frac{L_S}{2}\right)\right] \ddot{q}_{un}(t) \\ & + \rho_S A_S \int_0^{L_S} (U_S(z))^2 dz\, \ddot{q}_{us}(t) \\ & + \rho_S I_{Sxx} \sum_{n=1}^{\infty} \left[\int_0^{L_S} U_S'(z) U_n'(z) dz\right] \ddot{q}_{un}(t) \\ & + I_{Dzz}\Omega \sum_{even\ n}^{\infty} U_S'\left(\frac{L_S}{2}\right) U_n'\left(\frac{L_S}{2}\right) \dot{q}_{vn}(t) \\ & + \rho_S I_{Szz}\Omega \sum_{n=1}^{\infty} \left[\int_0^{L_S} U_S'(z) U_n'(z) dz\right] \dot{q}_{vn}(t) \\ & + E_S I_{Sxx} \int_0^{L_S} \left(U_S''(z)\right)^2 dz\, q_{us}(t) \\ & + k_b \left[(U_S(0))^2 + (U_S(L_S))^2\right] q_{us}(t) = 0\end{aligned} \tag{21}$$

And

$$\begin{aligned}& \sum_{odd\ n}^{\infty} \left[m_D U_S\left(\frac{L_S}{2}\right) U_n\left(\frac{L_S}{2}\right)\right] \ddot{q}_{vn}(t) \\ & + \sum_{even\ n}^{\infty} \left[I_{Dxx} U_S'\left(\frac{L_S}{2}\right) U_n'\left(\frac{L_S}{2}\right)\right] \ddot{q}_{vn}(t) \\ & + \rho_S A_S \int_0^{L_S} (U_S(z))^2 dz\, \ddot{q}_{vs}(t) \\ & + \rho_S I_{Sxx} \sum_{n=1}^{\infty} \left[\int_0^{L_S} U_S'(z) U_n'(z) dz\right] \ddot{q}_{vn}(t) \\ & - I_{Dzz}\Omega \sum_{even\ n}^{\infty} U_S'\left(\frac{L_S}{2}\right) U_n'\left(\frac{L_S}{2}\right) \dot{q}_{un}(t) \\ & - \rho_S I_{Szz}\Omega \sum_{n=1}^{\infty} \left[\int_0^{L_S} U_S'(z) U_n'(z) dz\right] \dot{q}_{un}(t) \\ & + E_S I_{Sxx} \int_0^{L_S} \left(U_S''(z)\right)^2 dz\, q_{vs}(t) \\ & + k_b \left[(U_S(0))^2 + (U_S(L_S))^2\right] q_{vs}(t) = 0\end{aligned} \tag{22}$$

The values of various parameters of the model are:

Table 4: Model Parameters

Parameters	Values
Rotational speed (Ω)	157.08 rad/s
Mass of disk (m_D)	10.654 kg
Mom. of iner. of disk (I_{Dxx})	210 $kgcm^2$
Pol. mom. of iner. of disk (I_{Dzz})	334 $kgcm^2$
Length of shaft (L_S)	519 mm
Density of shaft (ρ_S)	7860 kg/m^3
Cross-sec. of shaft (A_S)	8 cm^2
2nd mom. of area of shaft (I_{Sxx})	51472 mm^4
Pol. mom. of area of shaft (I_{Szz})	102944 mm^4
Elastic modulus of shaft (E_S)	202 GPa
Stiffness of bearing (k_b)	47487 kN/m

4. Results and Discussion

Taking three modes, the transverse displacements (14) become

$$\begin{aligned}u(z,t) = U_1(z)q_{u1}(t) + U_2(z)q_{u2}(t) + U_3(z)q_{u3}(t) \\ v(z,t) = U_1(z)q_{v1}(t) + U_2(z)q_{v2}(t) + U_3(z)q_{v3}(t)\end{aligned} \tag{23}$$

And the system's equations of motion (20) and (21) become

$$
\begin{aligned}
&m_{11}\ddot{q}_{u1}(t)+m_{13}\ddot{q}_{u3}+c_{11}\Omega\dot{q}_{v1}+c_{13}\Omega\dot{q}_{v3}+k_1q_{u1}=0\\
&m_{11}\ddot{q}_{v1}(t)+m_{13}\ddot{q}_{v3}-c_{11}\Omega\dot{q}_{11}-c_{13}\Omega\dot{q}_{u3}+k_1q_{v1}=0\\
&m_{22}\ddot{q}_{u2}(t)+c_{22}\Omega\dot{q}_{v2}+k_2q_{u2}=0\\
&m_{22}\ddot{q}_{v2}(t)-c_{22}\Omega\dot{q}_{u2}+k_2q_{v2}=0\\
&m_{31}\ddot{q}_{u1}(t)+m_{33}\ddot{q}_{u3}+c_{31}\Omega\dot{q}_{v1}+c_{33}\Omega\dot{q}_{v3}+k_3q_{u3}=0\\
&m_{31}\ddot{q}_{v1}(t)+m_{33}\ddot{q}_{v3}-c_{31}\Omega\dot{q}_{11}-c_{33}\Omega\dot{q}_{u3}+k_3q_{v3}=0
\end{aligned} \tag{24}
$$

where

$$
\begin{aligned}
&m_{11}=12.59;\ m_{13}=-13.11=m_{31};\\
&m_{22}=5.03;\ m_{33}=19.91\ kg;\\
&c_{11}=0.0071;\ c_{13}=-0.0142=c_{31};\\
&c_{22}=4.4916;\ c_{33}=0.0726\ kg;\\
&k_1=3.571;\ k_2=57.344;\ k_3=408.824\ MN/m
\end{aligned}
$$

Since the system of differential EOMs (24) are homogeneous linear ODEs with constant coefficients, the solutions are of the form [11]

$$
\begin{aligned}
&q_{u1}(t)=Q_{u1}e^{st};\ q_{u2}(t)=Q_{u2}e^{st};\ q_{u3}(t)=Q_{u3}e^{st};\\
&q_{v1}(t)=Q_{v1}e^{st};\ q_{v2}(t)=Q_{v2}e^{st};\ q_{v3}(t)=Q_{v3}e^{st}
\end{aligned} \tag{25}
$$

With the substitution of (25) into (24), the EOMs convert into

$$
\begin{aligned}
&(m_{11}s^2+k_1)Q_{u1}+m_{13}s^2Q_{u3}+c_{11}\Omega sQ_{v1}\\
&\quad+c_{13}\Omega sQ_{v3}=0\\
&-c_{11}\Omega sQ_{u1}-c_{13}\Omega sQ_{u3}+(m_{11}s^2+k_1)Q_{v1}\\
&\quad+m_{13}s^2Q_{v3}=0\\
&(m_{22}s^2+k_2)Q_{u2}+c_{22}\Omega sQ_{v2}=0\\
&-c_{22}\Omega sQ_{u2}+(m_{22}s^2+k_2)Q_{v2}=0\\
&m_{31}s^2Q_{u1}+(m_{33}s^2+k_3)Q_{u3}+c_{31}\Omega sQ_{v1}\\
&\quad+c_{33}\Omega sQ_{v3}=0\\
&-c_{31}\Omega sQ_{u1}-c_{33}\Omega sQ_{u3}+m_{31}s^2Q_{v1}\\
&\quad+(m_{33}s^2+k_3)Q_{v3}=0
\end{aligned} \tag{26}
$$

Since the first and the third modes are coupled and the second mode is independent of the two, the two systems must be independently solved. For the existence of non-trivial solution, the determinants of the two systems of (26) must separately vanish [11] resulting in following 4- and 8- degree equations in 's'.

$$
\begin{aligned}
&25.29\ s^4+(5.77*10^8+21.88\ \Omega)\ s^2+3.29*10^{15}=0\\
&and\ \ 6213\ s^8+8.23*10^{11}\ s^6+(2.75*10^{19}\\
&-9.97*10^{-8}\ \Omega)\ s^4+1.52*10^{25}\ s^2+2.13*10^{30}=0
\end{aligned} \tag{27}
$$

For the operating speed of 1500 rpm i.e. $\Omega=\dot{\psi}=157.08\ rad/s$, the roots of equation (27) are

$$
\begin{aligned}
&s_{1,2}=\pm3304.548j;\ s_{3,4}=\pm3450.671j\\
&s_{5,6}=\pm530.074j,\ s_{7,8}=\pm530.085j,\\
&s_{9,10}=\pm8118.523j,\ s_{11,12}=\pm8118.914j,
\end{aligned}
$$

so that $s=j\omega$

Therefore, the displacement solutions from (23) and (25) are

$$
\begin{aligned}
r(z,t)=&U_1(z)\sum_{p=5}^{8}Q_{r1p}e^{j\omega_pt}+U_2(z)\sum_{p=1}^{4}Q_{r2p}e^{j\omega_pt}\\
&+U_3(z)\sum_{p=9}^{12}Q_{r3p}e^{j\omega_pt}
\end{aligned}
$$

which can be written in the form of

$$
\begin{aligned}
r(z,t)=&U_1(z)\sum_{p=5,7}C_{r1p}\sin(\omega_pt+\lambda_p)\\
&+U_2(z)\sum_{p=1,3}C_{r2p}\sin(\omega_pt+\lambda_p)\\
&+U_3(z)\sum_{p=9,11}C_{r3p}\sin(\omega_pt+\lambda_p)
\end{aligned}
$$

So the natural frequencies of vibration in rad/s and Hz along with the critical speed in rpm for engine order(EO) of 16 are

Table 5: Analytical Results

Modes	$\omega(rad/s)$	$f(Hz)$	$N_{cr}(rpm)$
First (BW)	530.074	84.364	316.365
First (FW)	530.085	84.366	316.373
Second (BW)	3304.548	525.935	1972.256
Second (FW)	3450.671	549.191	2059.466
Third (BW)	8118.523	1292.103	4845.386
Third (FW)	8118.914	1292.165	4845.619

The results from modal analysis of ANSYS along with the deviation of analytical results from ANSYS results are given in table 6.

Table 6: ANSYS Results

Modes	$f(Hz)$	$N_{cr}(rpm)$	Error (%)
First (BW)	83.403	312.761	1.15
First (FW)	83.417	312.814	1.14
Second (BW)	456.490	1711.838	15.21
Second (FW)	486.420	1824.075	12.90
Third (BW)	1226.200	4598.250	5.37
Third (FW)	1226.500	4599.375	5.35

The plot of natural frequencies at different rotational speeds are shown in the following Campbell diagrams (9) to (11):

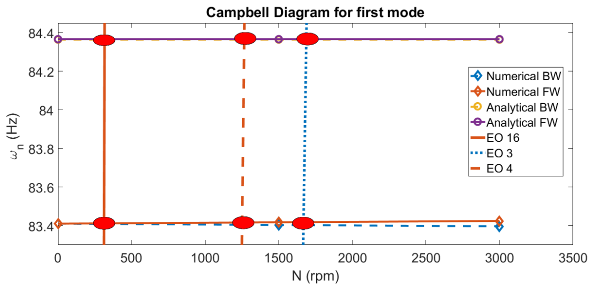

Figure 9: Variation of first mode natural frequency with rotational speed

Excitation line or Engine Order (EO) line intersects the natural frequency lines, the intersection being denoted by ellipses. The horizontal axis values of these ellipses correspond to the critical speed of the system [12]. Near 1500 r/min, EO of 3 and 4 are risky for the first mode so these EOs must be prevented.

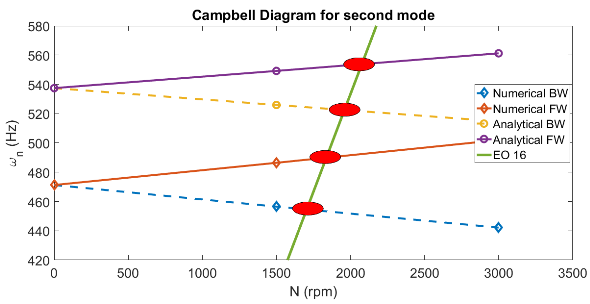

Figure 10: Variation of second mode natural frequency with rotational speed

For the given model, there are 16 buckets and EO of 16 crosses the first mode natural frequency near 300 r/min and the second mode near 2000 r/min. Even if 300 r/min may not be risky but speed range near 2000 r/min may be fatal for the system.

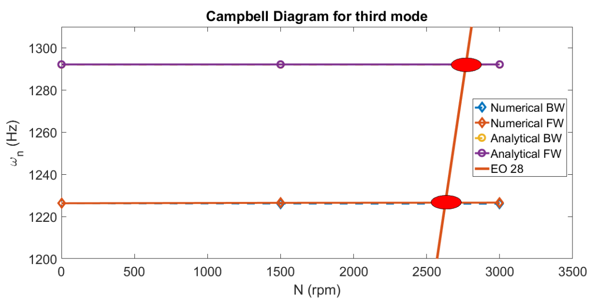

Figure 11: Variation of third mode natural frequency with rotational speed

The 16 EO line crosses the third mode line at speed higher than 3000 r/min. But EO of 28 due to number of rolling ball elements in each bearing crosses the third mode line near 2950 r/min.

The critical speeds from analytical model and numerical model corresponding to the EO of 16 have been provided in table (5) and (6). Table (6) gives the deviation of analytical results from numerical results implying that the critical speeds have been overestimated analytically.

5. Conclusion

The frequencies of vibration of central axis considering flexible rotor bearings at the support ends of the Pelton turbine are determined for the first three modes. At first mode, the freqecies are 530.074 rad/s and 530.085 rad/s corresponding to backward and forward whirl respectively. The corresponding values for the second mode are 3304.548 and 3450.671 while the values for the third mode are 8118.523 and 8118.914 rad/s. Different EO lines are passed from origin to find EO of 3 and 4 to be intersecting first mode frequency line at the operating speed. While EO encompassing 16 number of buckets intersects second mode near 2000 rpm respectively indicating the operation range near these speeds must be prevented avoiding possible failure of the system. Since, the 16 EO line doesn't intersect frequency line below 3000 r/min, the third mode critical frequency is high above the operating speed and is out of risk.

6. Acknowledgement

Authors are thankful to Department of Mechanical Engineering, Pulchowk Campus for providing continuous support during this work. Authors are very grateful to Incubation, Innovation and Entrepreneurship Center, Pulchowk Campus for providing the resources and guidance for the completion of this work. Authors would also like to thank Advanced College of Engineering and Management for making available time and resources required for this work.

References

[1] Pierre-Louis Viollet. From the water wheel to turbines and hydroelectricity. technological evolution and revolutions. *Comptes Rendus Mécanique*,

345(8):570 – 580, 2017. A century of fluid mechanics: 1870–1970.

[2] William Tyrrell Thomson and Marie Dillon Dahleh. *Theory of vibrations with applications*. Prentice Hall, 1st edition, 1993.

[3] Santosh Shelke. A review on dynamic analysis of pelton wheel turbine. 06 2016.

[4] Michel Lalanne and Guy Ferraris. *Rotordynamics prediction in engineering*, volume 2. Wiley, 1998.

[5] Rajiv Tiwari. *Rotor Systems: Analysis and Identification*. 12 2017.

[6] Singiresu S Rao and Fook Fah Yap. *Mechanical vibrations*, volume 4. Prentice hall Upper Saddle River, 2011.

[7] Arthur W Leissa and Mohamad S Qatu. *Vibrations of Continuous Systems*. McGraw-Hill, 2011.

[8] Laxman Motra and Mahesh Chandra Luintel. Free vibration analysis of selected pelton turbine using dynamic approach. In *Proceedings of IOE Graduate Conference*, volume 5, pages 229–236, 2017.

[9] S Graham Kelly. *Advanced vibration analysis*. CRC Press, 2006.

[10] S Graham Kelly. *Mechanical vibrations: theory and applications*. Cengage learning, 2012.

[11] Erwin Kreyszig. Advanced engineering mathematics, 8-th edition, 1999.

[12] Meherwan P Boyce. *Gas turbine engineering handbook*. Elsevier, 2011.